J. Fluid Mech. (1990), *vol.* 220, *pp.* 293–307
Printed in Great Britain

Instability waves in twin supersonic jets

By PHILIP J. MORRIS

Department of Aerospace Engineering, Penn State University, University Park, PA 16802, USA

(Received 15 September 1989)

Calculations are presented for the characteristics of instability waves in the initial mixing region of twin circular supersonic jets. Two models for the basic jet flow are used. In the first, the jets are modelled as two circular vortex sheets. In the second, realistic velocity and density profiles are used. It is shown that the unsteady flow fields of the two jets interact before the time-averaged jets flows have merged. The normal modes or instability waves are classified by their symmetry properties in the twin-jet case and their asymptotic behaviour for large jet separations. Calculations of the growth rates and phase velocities are made for these modes as a function of jet separation and mixing-layer thickness. The associated pressure distributions are also presented. In the realistic jet profile calculations the effect of jet separation is found to be relatively weak. For modes that are even about the symmetry plane between the two jets the pressure levels are found to increase near this plane as the jet separation decreases.

1. Introduction

When supersonic jets from convergent–divergent nozzles operate at off-design conditions they can produce intense screech tones. Powell (1953) made early observations of this phenomenon and proposed a feedback mechanism for the screech tone production. More recent experiments and analysis by Tam, Seiner & Yu (1986) showed that the feedback loop consists of downstream-propagating large-scale structures in the jet mixing layer that interact with the shock cell structure to generate upstream-travelling acoustic waves. If these acoustic waves trigger additional flow disturbances at the jet lip with the correct phase then the feedback loop is established. Analyses, based on this model, have made excellent predictions of screech tone frequencies in both circular and non-circular jets; see Tam (1986) and Morris, Bhat & Chen (1989).

Seiner, Manning & Ponton (1988) showed experimentally that for two closely spaced supersonic jets, operating off-design, the dynamic loads associated with the screech tone can reach levels, upstream of the jets' exits, that could result in structural damage. Tam & Seiner (1987) noted that the screech tone frequency of the twin jets was slightly different to that of the single jet and that the acoustic intensity in the internozzle region exceeded that of the direct sum of two non-interacting screeching jets. This suggests that there is a strong interaction between the unsteady flow and acoustic fields of the two jets. The analysis and calculations described in this paper help to quantify the effects of jet separation and operating conditions on the nature of this interaction.

Turbulent mixing in free shear flows is controlled by the dynamics of large-scale coherent structures. The local characteristics of these structures may be described by

linear instability theory. This has been demonstrated by the experiments of Gaster, Kit & Wygnanski (1985), and Petersen & Samet (1988) among others. In their experiments they compared predictions of the amplitude and phase of the axial velocity fluctuations, based on linear stability theory, with phase-averaged measurements in an excited shear layer and a jet. The agreement between predictions and experiment was very good though only the local distributions and not the amplitude were predicted. This close agreement between the predictions of linear stability thoery and the properties of the large-scale coherent structures has formed the basis for theories of turbulent mixing and supersonic jet noise. For example, Tam & Morris (1980), and Tam & Burton (1984*a*, *b*) predicted the noise radiation from instability waves in supersonic shear layers and jets and obtained very good agreement with experiment.

For supersonic jets the three main components of noise radiation are turbulent mixing noise, broadband shock-associated noise and screech. In each case, the essential component of the turbulence responsible for noise generation is the large-scale structures. It should be noted that this is not the case for subsonic jets where a complete theory for noise generation and radiation is not available. Tam (1987) showed how predictions could be made for each noise component in a supersonic circular jet using an instability wave model for the large-scale structures.

In the present paper the properties of the instability waves or large-scale turbulent structures in the initial mixing region of twin circular supersonic jets are determined. Two models for the basic jet flows are used. In the first, the jets are modelled as two circular vortex sheets. In the second, realistic mean velocity and density profiles are used. Though the former model fails to provide quantitative results it does help to explain the observed modes of instability and interactions predicted by the more realistic model. The calculations examine whether the instability growth rates, and hence the amplitudes of the large-scale structures, are modified as the jet separation and operating conditions vary. In addition, the corresponding changes in the instability wave phase velocity are predicted. It is shown that the unsteady flow fields associated with the instability waves do interact before the time-averaged jet flows have merged. However, this interaction is relatively weak for the operating conditions considered. In §2 the general equations of motion and analytic solutions common to both models are developed. The details of the vortex sheet model and its predictions are then described in §3. Section 4 contains the numerical procedures and calculations for the realistic jet profiles. Finally, the role of these predictions in and their relationship to experimental observations of the twin-plume resonance phenomenon are discussed.

2. Analysis

Consider the two circular jets shown in figure 1. The time-averaged jet flows are assumed to be symmetric about the (x, z)- and (x, y)-planes, where the x-coordinate is normal to the jet exit planes. The centres of the jets are separated by a distance $2h$. Throughout this analysis the variables are non-dimensionalized with respect to the jet velocity u_j, jet density ρ_j and jet radius a_j. These values are taken to be the fully expanded jet properties as defined by Tam & Tanna (1982). These values are described below. In the annular mixing regions of the two jets, before they have merged, there are three flow regions. In region (i), the potential cores of the jets, the mean velocity and density are constant. Region (iii) represents the stationary fluid surrounding the jets. In region (ii), the annular mixing region, the mean velocity $\bar{u}$

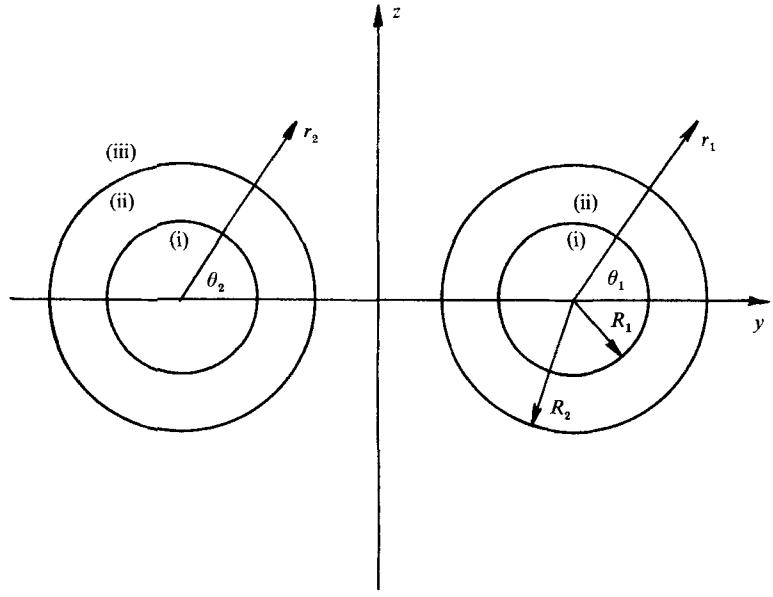

FIGURE 1. Schematic of twin-jet cross-section and coordinate systems.

and density $\bar{\rho}$ are variable. Polar coordinate systems are introduced (r_1, θ_1) and (r_2, θ_2) with origins on the jet centrelines. The mean velocity and density of each jet are assumed to be a function of their radial coordinates only. This is the locally parallel flow approximation. The potential cores have radii R_1 and the outer edges of the mixing regions have radii R_2. The mean static pressure is assumed to be constant. The large-scale coherent structures are modelled as instability waves. Their behaviour is governed by the unsteady, linearized, compressible equations of motion. Thus, for example, in either polar coordinate system separable solutions for the pressure fluctuation are sought in the form

$$p(\boldsymbol{x}, t) = \hat{p}(r) \exp[\mathrm{i}(kx + n\theta - \omega t)], \tag{2.1}$$

where k is an axial wavenumber, n is an azimuthal mode number, and ω is a radian frequency. The radial variation of the pressure fluctuation is then found to satisfy the equation

$$\frac{\mathrm{d}^2\hat{p}}{\mathrm{d}r^2} + \left\{\frac{1}{r} - \frac{1}{\bar{\rho}}\frac{\mathrm{d}\bar{\rho}}{\mathrm{d}r} + \frac{2k}{\Omega}\frac{\mathrm{d}\bar{u}}{\mathrm{d}r}\right\}\frac{\mathrm{d}\hat{p}}{\mathrm{d}r} + \left\{k^2 - \bar{\rho}\Omega^2 M_\mathrm{j}^2 + \frac{n^2}{r^2}\right\}\hat{p} = 0, \tag{2.2}$$

where

$$\Omega = \omega - k\bar{u},$$

and $M_\mathrm{j}^2 = u_\mathrm{j}^2/c_\mathrm{j}^2$, where c_j is the fully expanded jet speed of sound. Equation (2.2) reduces to Bessel's equation in regions of constant mean velocity and density.

A solution for the pressure fluctuations outside the jet mixing layers in region (iii) may be obtained in either polar coordinate system in the form

$$p(r, \theta, x, t) = \sum_{n=-\infty}^{\infty} B_n H_n^{(1)}(\mathrm{i}\lambda_0 r) \exp[\mathrm{i}(kx - \omega t + n\theta)], \tag{2.3}$$

where

$$\lambda_0 = \{k^2 - \bar{\rho}_0 \omega^2 M_\mathrm{j}^2\}^{\frac{1}{2}}.$$

$\bar{\rho}_0$ is the non-dimensional mean density in the ambient medium which is equal to the jet static temperature ratio, T_j/T_0. The branch cuts for λ_0 are chosen such that

$$-\tfrac{1}{2}\pi \leqslant \arg \lambda_0 < \tfrac{1}{2}\pi.$$

This ensures that the solutions decay as $r \to \infty$ or are outgoing waves, for positive frequency. The symmetry properties of the mean velocity and density field, for example

$$\bar{u}(y, z) = \bar{u}(-y, z) = \bar{u}(y, -z),$$

indicate that the eigensolutions should be odd or even about the (x, y)- and (x, z)-planes. From the latter symmetry property (the former symmetry property is used below) the general solution for the pressure fluctuations in the outer region may be written

$$p(r_1, r_2, \theta_1, \theta_2, x, t) = \sum_{n=-\infty}^{\infty} B_n \{H_n^{(1)}(\mathrm{i}\lambda_0 r_2) \exp(\mathrm{i}n\theta_2) \pm H_n^{(1)}(\mathrm{i}\lambda_0 r_1) \exp[\mathrm{i}n(\pi - \theta_1)]\} \exp[\mathrm{i}(kx - \omega t)], \quad (2.4)$$

where the choice of sign depends on whether the solution is to be odd or even about the (x, z)-plane of symmetry.

It should be noted that this solution does not just represent the sum of the contributions from two, non-interacting, individual jets, though the form could then be the same. It is simply a convenient form of the separable solution in the outer region. The influence of the second jet is included when this general form of outer solution is matched with the solution in the interior of each jet. In the present case the fluctuations in each jet are affected not only by the outgoing solutions that would exist for an individual, isolated jet, but also by the incoming solutions from the second jet. These two contributions are included in the outer solution (2.4).

In order to match the outer solution (2.4) with the pressure fields in regions (i) and (ii) it is convenient to write the solutions in region (iii) in terms of only one of the two polar coordinate systems. This may be accomplished using Graf's Addition Theorem (see Tranter 1968). For example, we may write

$$H_n^{(1)}(\mathrm{i}\lambda_0 r_1) \exp[\mathrm{i}n(\pi - \theta_1)] = \sum_{s=-\infty}^{\infty} H_{n+s}^{(1)}(2\mathrm{i}\lambda_0 h) J_s(\mathrm{i}\lambda_0 r_2) \exp(\mathrm{i}s\theta_2). \quad (2.5)$$

Then (2.4) may be written

$$p(r_2, \theta_2) = \sum_{n=-\infty}^{\infty} \exp(\mathrm{i}n\theta_2) \sum_{s=-\infty}^{\infty} B_s \beta_{sn}(\mathrm{i}\lambda_0 r_2), \quad (2.6)$$

where

$$\beta_{sn}(\xi) = \delta_{sn} H_s^{(1)}(\xi) \pm H_{n+s}^{(1)}(2\mathrm{i}\lambda_0 h) J_n(\xi), \quad (2.7)$$

and δ_{sn} is the Kronecker delta function. It should be noted that

$$\beta_{-s,-n} = (-1)^s \beta_{sn}, \quad (2.8a)$$

and

$$\beta_{-s,n} = (-1)^s \beta_{s,-n}. \quad (2.8b)$$

The influence of the second jet is seen in (2.7). The first term on the right-hand side represents the outgoing waves from the jet at $y = -h$. The second term represents the incoming waves from the jet at $y = h$. For large h this latter term is very small and the interaction between the jets is very weak.

The normal modes for the pressure fluctuation given by (2.6) may be separated further into modes that are odd or even about the (x, y)-plane. This is accomplished

by first setting $s = -s$ and $n = -n$ and adding the resulting equation to (2.6). Then the pressure fluctuation may be written

$$p(r_2, \theta_2) = \sum_{n=-\infty}^{\infty} \sum_{s=-\infty}^{\infty} [F_s \cos(n\theta_2) + \mathrm{i} G_s \sin(n\theta_2)] \beta_{sn}(\mathrm{i}\lambda_0 r_2), \tag{2.9}$$

where
$$F_s = \tfrac{1}{2}[B_s + (-1)^s B_{-s}], \tag{2.10a}$$

and
$$G_s = \tfrac{1}{2}[B_s - (-1)^s B_{-s}]. \tag{2.10b}$$

A similar solution may be found for the pressure fluctuations in the potential core region. This may be written

$$p(r_2, \theta_2) = \sum_{n=-\infty}^{\infty} [A_n \cos(n\theta_2) + \mathrm{i} C_n \sin(n\theta_2)] J_n(\mathrm{i}\lambda_1 r_2), \tag{2.11}$$

where
$$\lambda_1^2 = k^2 - (\omega - k)^2 M_j^2. \tag{2.12}$$

With the form of the solutions known inside and outside the jet the eigenvalues k may be determined by matching these solutions at either the vortex-sheet location or through the finite mixing layer. The former matching is described in the next section.

3. Vortex-sheet model

3.1. *Analysis*

In this representation of the jet flows the finite mixing layers are replaced by cylindrical vortex sheets of unit non-dimensional radius. Across the vortex sheet we require continuity of pressure and particle displacement. The matching conditions require that

$$\Delta\left[\frac{\mathrm{d}p/\mathrm{d}r_2}{\bar{\rho}\Omega^2}\right] = 0, \quad \Delta[p] = 0, \tag{3.1}$$

where $\Delta[\ ]$ denotes the change in the argument across the vortex sheet. If the interior solutions given by (2.11) are matched with the exterior solutions, (2.9), for all n we obtain, for the solutions that are even about the (x, y)-plane,

$$\sum_{s=\infty}^{\infty} F_s\{\bar{\rho}_a \omega^2 \lambda_1 J_n'(\mathrm{i}\lambda_1) \beta_{sn}(\mathrm{i}\lambda_0) - (\omega - k)^2 \lambda_0 J_n(\mathrm{i}\lambda_1) \beta_{sn}'(\mathrm{i}\lambda_0)\} = 0, \quad n = -\infty, \ldots, \infty, \tag{3.2}$$

where
$$\beta_{sn}'(\xi) = \delta_{sn} H_s^{(1)\prime}(\xi) \pm H_{n+s}^{(1)}(2\mathrm{i}\lambda_0 h) J_n'(\xi). \tag{3.3}$$

If we use the symmetry properties of β_{sn}, given by (2.8), and note that

$$F_s = (-1)^s F_{-s}, \tag{3.4}$$

then the independent equations yielded by (3.2) may be written

$$\sum_{s=1}^{\infty} F_s\{\Gamma_n \delta_{sn} \pm [H_{n+s}^{(1)}(2\mathrm{i}\lambda_0 h) + (-1)^s H_{n-s}^{(1)}(2\mathrm{i}\lambda_0 h)]\}$$
$$+ F_0\{\Gamma_n \delta_{0n} \pm H_n^{(1)}(2\mathrm{i}\lambda_0 h)\} = 0, \quad n = 0, 1, \ldots, \infty, \tag{3.5}$$

where
$$\Gamma_n = \frac{H_n^{(1)}(\mathrm{i}\lambda_0) - \Lambda_n H_n^{(1)\prime}(\mathrm{i}\lambda_0)}{J_n(\mathrm{i}\lambda_0) - \Lambda_n J_n'(\mathrm{i}\lambda_0)} \tag{3.6}$$

and
$$\Lambda_n = \frac{(\omega - \alpha)^2 \lambda_0 J_n(\mathrm{i}\lambda_1)}{\bar{\rho}_0 \omega^2 \lambda_1 J_n'(\mathrm{i}\lambda_1)}. \tag{3.7}$$

In the numerical calculations the series is truncated at $s = N$ and then (3.5) yields a set of $N+1$ homogeneous equations for F_s. These may be written in matrix form,

$$[\boldsymbol{A}]\boldsymbol{F} = \boldsymbol{0}, \tag{3.8}$$

where $\boldsymbol{F}$ is a vector of length $N+1$ of the unknown coefficients F_s. For a non-trivial solution to exist the determinant of this matrix must be zero. This provides the dispersion relationship between the wavenumber and frequency.

A similar set of equations may be derived for the unknown coefficients in the series representing the solutions that are odd about the (x, y)-plane. These may be written as in (3.4):

$$F_s = (-1)^s F_{-s};$$

then the independent equations yielded by (3.2) may be written

$$\sum_{s=1}^{\infty} G_s\{\Gamma_n \delta_{sn} \pm [H^{(1)}_{n+s}(2\mathrm{i}\lambda_0 h) + (-1)^s H^{(1)}_{n-s}(2\mathrm{i}\lambda_0 h)]\} = 0, \quad n = 0, 1, \ldots, \infty. \tag{3.9}$$

The requirement of a non-trivial solution for G_s results in a dispersion relationship for the odd modes about the (x, y)-plane.

A similar expression to both (3.5) and (3.9) was obtained by Sedel'nikov (1967). He developed dispersion relationships for multilayer jets, several jets, and jets between parallel walls or in rectangular ducts. In each case the jet was represented by a vortex sheet. No roots of the dispersion relationship were determined. Written in the form of (3.5) and (3.9) the off-diagonal elements vanish for large jet separations and the eigenvalues are the zeroes of Γ_n. These eigenvalues correspond to the axisymmetric and helical normal modes of a single jet.

It is clear that this form of the equations does not hold for zero frequency. This case is of interest, as it may be used in a description of the shock cell structure of the jet. Tam & Tanna (1982) showed how a model for the shock cell structure could be posed as an initial-value problem in which the fully expanded vortex sheet acts as a waveguide for the pressure perturbation at the jet exit. For the steady problem the matching conditions at the vortex sheet require that the pressure perturbation be zero at and outside the vortex sheet. Thus there is no communication between the two jets and the shock cell structure remains unchanged from the single-jet case. However, it should be noted that this is only true for jets into stationary air and some coupling between the steady shock cell structure could occur if the ambient air were in motion; see Morris (1988).

3.2. *Calculations*

There are many parameters and operating conditions that could be varied for the present configuration. Thus, the calculations have been limited to a set of operating conditions that correspond to available experiments. In the calculations for both the vortex sheet and the realistic mean profile representation of the jet, the diameter of the jet is taken to be the fully expanded jet diameter. It may be argued that in the case of either an over- or under-expanded jet, the jet plume will adjust its cross-section so as to preserve mass flux but equalize the mean static pressure. This gives the following relationship, assuming isentropic flow, between the fully expanded and design jet dimensions:

$$r_{\mathrm{d}} = \left(\frac{M_{\mathrm{j}}}{M_{\mathrm{d}}}\right)^{\frac{1}{2}} \left\{\frac{1+\frac{1}{2}(\gamma-1)M_{\mathrm{d}}^2}{1+\frac{1}{2}(\gamma-1)M_{\mathrm{j}}^2}\right\}^{\frac{\gamma+1}{4(\gamma-1)}}, \tag{3.10}$$

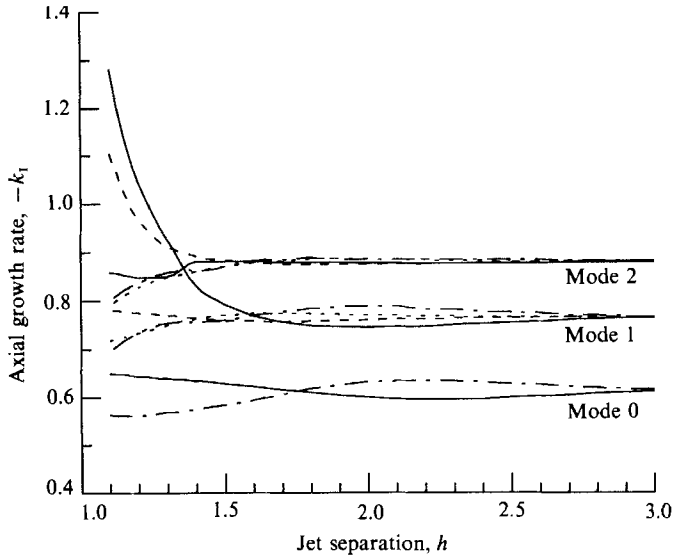

FIGURE 2. Variation of the axial growth rate $-k_I$ with jet spacing. $M_j = 1.32$, $M_d = 1.0$, $St = 0.318$. ——, mode type I; – – – –, type II; — — —, type III; ....., type IV.

(x, y)-plane	(x, z)-plane	Mode
Even	Even	I
Odd	Even	II
Even	Odd	III
Odd	Odd	IV

TABLE 1. Classification of normal modes

where r_d is the non-dimensional design jet radius and M_j and M_d are the fully expanded and design jet Mach numbers respectively.

The instability wave calculations in the vortex-sheet case provide an indication of the character of the results to be expected in the more realistic calculations that include the effects of finite mixing-layer thickness. Four types of solution may be classified as shown in table 1. In addition, each solution may be classified by the azimuthal mode number it approaches as the jets move further apart.

Figure 2 shows the variation of the axial growth rate, $-k_I$ as a function of the separation distance between the two jets' centrelines h. The instability wave frequency is 1.0 in each case. This corresponds to a Strouhal number of 0.318, $(1/\pi)$, based on the fully expanded jet diameter and velocity. The design and fully expanded jet Mach numbers are 1.0 and 1.32 respectively and the jet is unheated. These conditions correspond to the experiments of Seiner *et al.* (1988). In the numerical evaluation of the dispersion relationships obtained from (3.5) and (3.9) a value of $N = 5$ was used. Calculations were also performed with $N = 9$ with no significant change, even for small values of jet separation. For large separations the solutions approach those for the single jet and the growth rate increases with azimuthal mode number. Calculations are presented for mode numbers 0, 1 and 2. For a given mode number the most unstable mode type is a function of jet spacing. For example, consider the mode number 1. For $h > 1.6$ the type III mode is the

most unstable, though its value does not differ greatly from the value at large h. For $h < 1.6$ the type I mode dominates. For the range of mode numbers and types considered, the mode number 1, type I mode appears to be most affected by small separations, showing a large increase in axial growth rate. This mode is associated with a motion that is even about both (x, y)- and (x, z)-planes and is dominated by a pair of helical motions of opposite sense about each jet. This is the type B mode described by Seiner *et al.* (1988) which they found to be the dominant mode in their twin-plume resonance experiments.

The prediction that the stability of the (1, I) mode is affected strongly by the jet separation and the interchange of dominance between modes of different types as the jet separation changes is encouraging, as it provides qualitative agreement with the observations of Seiner *et al.* (1988) and Wlezian (1987). However, these results should be treated with some caution as they are based on the vortex-sheet model for the jet. The dominant or preferred mode of a real jet is determined by the total growth of a given frequency disturbance through the developing shear layer. In the next section more realistic profiles are used to describe the jet flow.

4. Realistic jet flow model

4.1. *Analysis*

In this case the mean velocity and density vary in region (ii) in a smooth, realistic manner. The matching between the potential core and ambient flow solutions must be performed using a numerical solution in the mixing layer.

In the potential core the solution for the pressure fluctuation takes the form given by (2.11). Consider, for example the modes that are even about the (x, y)-plane. For $n = -\infty, \ldots, \infty$ (2.2) may be integrated from $r = R_1$ to $r = R_2$ with initial conditions

$$\hat{p} = J_n(\mathrm{i}\lambda_1 R_1), \quad \frac{\mathrm{d}\hat{p}}{\mathrm{d}r} = \mathrm{i}\lambda_1 J_n'(\mathrm{i}\lambda_1 R_1). \tag{4.1}$$

The corresponding numerical solutions at $r = R_2$ are denoted by $\hat{p}_n$ and $\hat{p}_n'$. These solutions may be matched with the exterior solutions for all n. That is,

$$A_n p_n = \sum_{s=-\infty}^{\infty} F_s \beta_{sn}(\mathrm{i}\lambda_0 R_2), \tag{4.2}$$

and

$$A_n \hat{p}_n' = \sum_{s=-\infty}^{\infty} \mathrm{i}\lambda_0 F_s \beta_{sn}'(\mathrm{i}\lambda_0 R_2). \tag{4.3}$$

Following the same approach as used in §3, based on the symmetry properties of $\hat{p}_n$, β_{sn} and F_s, a dispersion relationship may be derived from an identical system of equations to (3.5). However, in this case the Γ_n and Λ_n are defined by

$$\Gamma_n = \frac{H_n^{(1)}(\mathrm{i}\lambda_0 R_2) - \Lambda_n H_n^{(1)\prime}(\mathrm{i}\lambda_0 R_2)}{J_n(\mathrm{i}\lambda_0 R_2) - \Lambda_n J_n'(\mathrm{i}\lambda_0 R_2)} \tag{4.4}$$

and

$$\Lambda_n = \mathrm{i}\lambda_0 \hat{p}_n / \hat{p}_n'. \tag{4.5}$$

For modes that are odd about the (x, y)-plane the dispersion relationship may be obtained from (3.9) with Γ_n and Λ_n defined by (4.4) and (4.5) respectively.

4.2. *Calculations*

In the subsequent calculations it is assumed that the mean velocity and density of the jet flows take the same form as in the single-jet case: up to the location where the jet edges meet. The mean velocity is assumed to take the form

$$\bar{u}(r,x) = \begin{cases} 1, & r \leqslant g(x) \\ \exp[-\ln(2)\,\eta^2], & r > g(x), \end{cases} \tag{4.6}$$

where

$$\eta = [r - g(x)]/b(x). \tag{4.7}$$

$g(x)$ is the radius of the potential core and $b(x)$ is the half-width of the mixing layer.

The mean density is related to the mean velocity through a Crocco relationship,

$$\bar{\rho} = [\tfrac{1}{2}(\gamma-1)\,\bar{u}(1-\bar{u})M_j^2 + \bar{u} + T_0'(1-\bar{u})]^{-1}, \tag{4.8}$$

where T_0' is the non-dimensional ambient temperature.

From the mean axial momentum integral equation a relationship may be found between the potential core radius and the half-width of the mixing layer:

$$g(x) = -\beta_1 b + (b^2(\beta_1^2 - 2\beta_2) + 1)^{\frac{1}{2}}, \tag{4.9}$$

where

$$\beta_1 = \int_0^\infty \bar{\rho}\bar{u}^2\,\mathrm{d}\eta,$$

and

$$\beta_2 = \int_0^\infty \bar{\rho}\bar{u}^2\eta\,\mathrm{d}\eta.$$

At some axial location the edges of the two jets will touch on the symmetry plane and the present analysis, which assumes that the mean flow is axisymmetric relative to each jet's centreline, is no longer valid. In the present calculations the edge of the jet is taken to be the location at which the axial velocity given by (4.6) equals 0.01. This corresponds to a value of η of 2.58. Thus the present calculations are for values of jet thickness such that

$$g(b) + 2.58b \leqslant h. \tag{4.10}$$

A variable-step-size fourth-order Runge–Kutta algorithm is used to integrate (2.2) from the edge of the potential core to $\eta = 2.58$. This gives the values of $\hat{p}_n$ and $\hat{p}_n'$. As in the vortex-sheet calculations the upper limit in the series representations is taken to be $N = 5$. Calculations have also been performed with $N = 9$ with negligible change in the largest elements of F_s or G_s.

The vortex-sheet calculations, shown in figure 2, indicate that for large separations the higher azimuthal mode numbers have higher axial growth rates. Additional calculations show that, for the present operating conditions, the maximum axial growth rate occurs for $n = 3$. A similar result is obtained for small values of local thickness $b(x)$. However, as the jet mixing-layer thickens, the higher-order azimuthal modes become damped more quickly. Figure 3 shows the variation of the axial growth rate $-k_{\mathrm{I}}$ as a function of thickness $b(x)$ for a large jet separation $h/r_{\mathrm{d}} = 5.0$, for the first three azimuthal modes. In this and subsequent calculations the fully expanded jet Mach number is 1.32, the design jet Mach number is 1.0, and the jet is unheated. Figure 3 shows how the growth rate of the $n = 2$ mode rapidly decreases. The helical mode $n = 1$ has a larger growth rate than the axisymmetric mode $n = 0$ for all the values of jet thickness considered. In the subsequent calculations only the two lowest mode numbers will be examined. The calculations shown in figure 3 give results that are identical to the single-jet case.

As the separation decreases, the growth rates of the various mode numbers and types move away from their large-separation value. Figure 4 shows this variation for

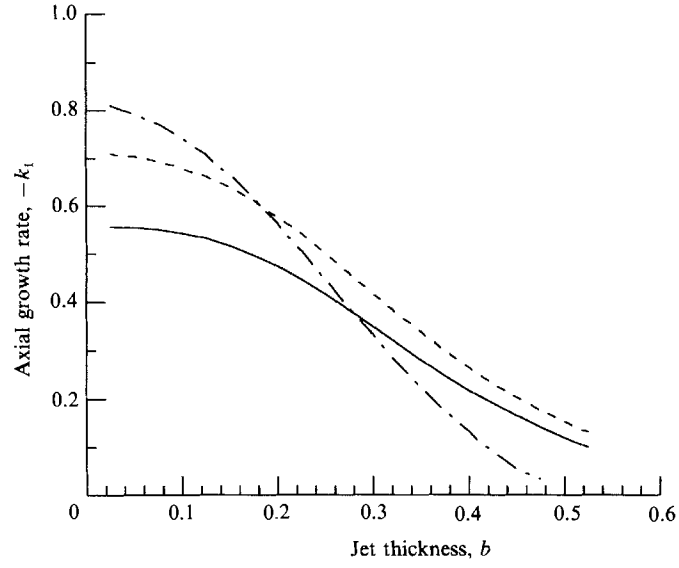

FIGURE 3. Variation of the axial growth rate $-k_i$ with jet mixing-layer thickness. $M_j = 1.32$, $M_d = 1.0$, $St = 0.3$, $h/r_d = 5.0$. ——, $n = 0$; – – – –, $n = 1$; — — —, $n = 2$.

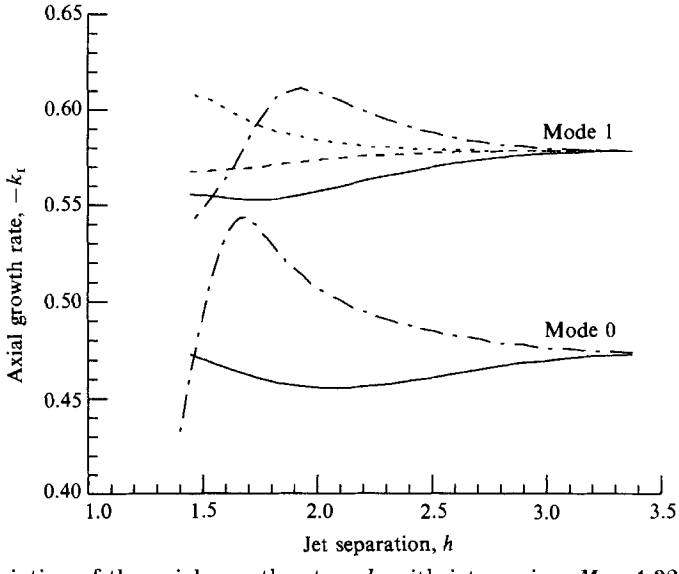

FIGURE 4. Variation of the axial growth rate $-k_i$ with jet spacing. $M_j = 1.32$, $M_d = 1.0$, $St = 0.3$, $b = 0.2$. ——, mode type I; – – – –, type II; — — —, type III; ....., type IV.

mode numbers 0 and 1 and the four mode types. The jet thickness is $b = 0.2$ and the Strouhal number $St = 0.3$. The change in the axial growth rate is relatively small for jet separations greater than 2 radii. For these conditions the most unstable mode at the closest separation achievable, before the jets' edges merge, is the (1, IV) mode. This mode is dominated by two helical instabilities that are out of phase that give a solution that is odd about both the (x, y)- and (x, z)-planes. However, at other separations other modes are the most unstable.

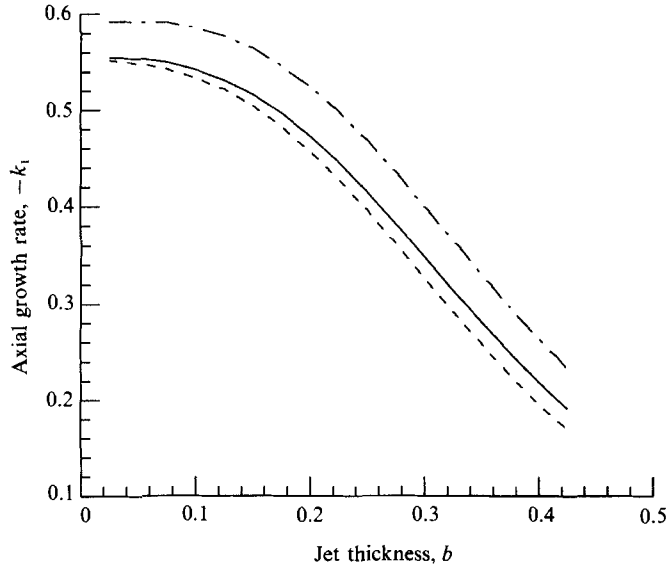

FIGURE 5. Variation of the axial growth rate $-k_I$ with jet mixing-layer thickness. $M_j = 1.32$, $M_d = 1.0$, $St = 0.3$. ——, $n = 0$, $h/r_d = 5.0$; – – –, (0, I), $h/r_d = 1.9$; ——, (0, III), $h/r_d = 1.9$.

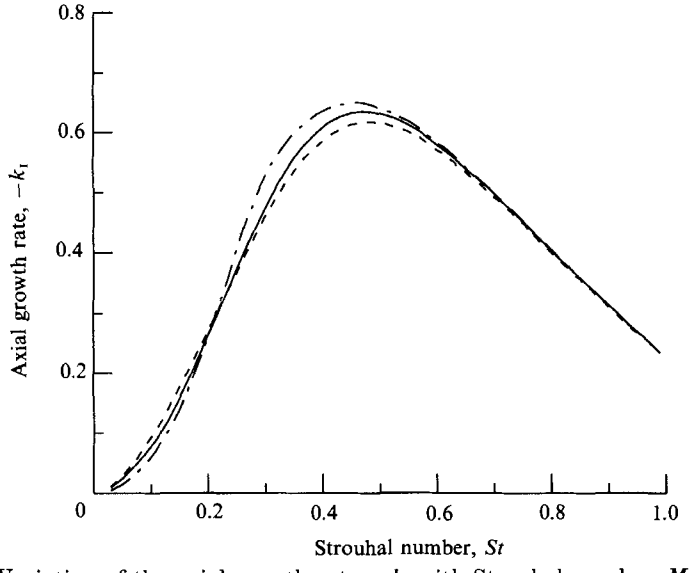

FIGURE 6. Variation of the axial growth rate $-k_I$ with Strouhal number. $M_j = 1.32$, $M_d = 1.0$, $b = 0.2$. For legend see figure 5.

The relative instability of the various modes at a given separation has been found to be nearly independent of jet mixing-layer thickness. For example, figure 5 shows the variation of axial growth rate with $b(x)$ for the (0, I) and (0, III) modes. The single-jet, $n = 0$ value is shown for comparison. In this case, with $h/r_d = 1.9$, the (0, III) mode is the most unstable at all jet thicknesses.

Before considering the eigenfunctions for the various modes of instability, the effect of wave frequency will be considered. Figure 6 shows the variation of axial growth rate $-k_I$ with Strouhal number for the same modes as shown in figure 5. The

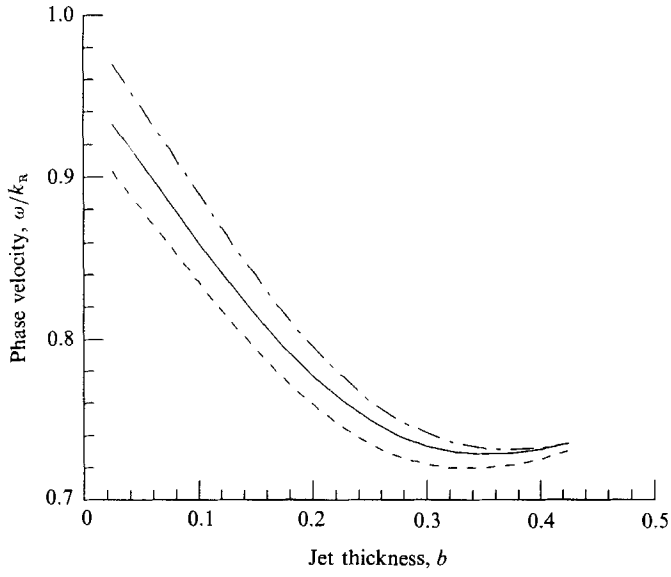

FIGURE 7. Variation of the phase velocity, ω/k_R, with jet mixing layer thickness. $M_j = 1.32$, $M_d = 1.0$, $St = 0.3$. For legend see figure 5.

mixing-layer thickness $b = 0.2$. Except for the lower Strouhal numbers the (0, III) mode is more unstable than the (0, I) mode or the $n = 0$ single-jet mode. At this jet thickness the most unstable frequency occurs for a Strouhal number of approximately 0.45 and is relatively independent of jet separation or mode type.

The real part of the wavenumber is also affected by the jet separation. The trend in all the cases considered involves an increase in k_R for the even modes about the (x, z)-plane and a decrease in k_R for the odd modes as the jet separation decreases. However, the changes are relatively small, involving typically a 10% change from the single-jet value. For example, figure 7 shows the variation with mixing-layer thickness of the phase velocity, given by ω/k_R, for the same modes as shown in figure 5. The phase velocity for the (0, I) mode,which is even about the (x, z)-plane, is lower than the single-jet or large-separation value. Conversely, the (0, III) mode, which is odd about the (x, z)-plane, takes a higher value. It should be noticed that for larger thicknesses, where the instability wave is reaching its maximum amplitude or neutrally stable condition, there is effectively no change in the phase velocity. In this region the phase velocity is approximately 0.73. Thus the observed shift in the screech frequency for the twin jets is linked to a change in the shock cell spacing rather than a modification to the phase velocity of the large-scale structures. Seiner *et al.* (1988) did observe a 10–15% increase in the shock cell spacing. The reason for this increase is unclear as, in the absence of ambient flow, the shock cell structure of the two jets should be independent. However, insufficient aerodynamic data for the twin jets are available at present to help to explain this observation.

The pressure distributions associated with each mode of instability may be constructed by obtaining the coefficients F_s or G_s for a given eigenvalue. An inverse iteration technique is used to obtain these values. That is,

$$[\boldsymbol{A}]\,\boldsymbol{F}^{k+1} = \sigma \boldsymbol{F}^{k}, \tag{4.11}$$

where σ is a scaling factor and $[\boldsymbol{A}]$ is given by (3.8). An initial guess for $\boldsymbol{F}^0$ is taken to be $\{1, 1, \ldots, 1\}^{\mathrm{T}}$. This algorithm has been found to give convergence in two

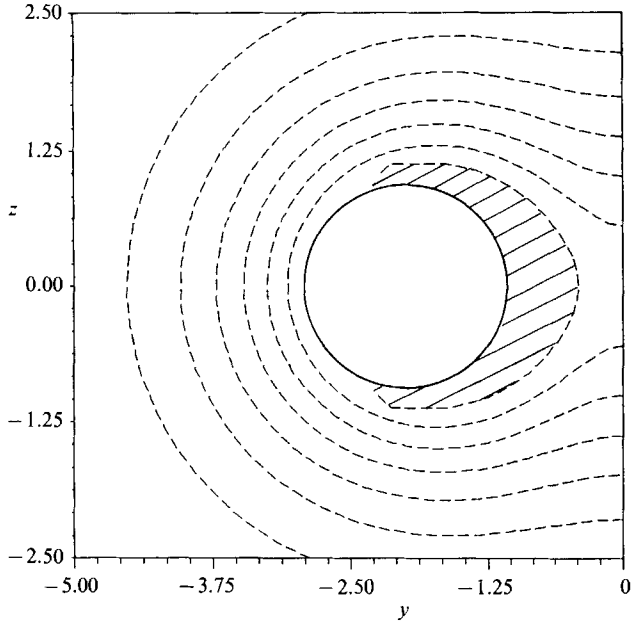

FIGURE 8. Contours of equal pressure level, Mode (0, I). $M_j = 1.32$, $M_d = 1.0$, $St = 0.3$, $h/r_d = 1.9$. ——, outer edge of the jet. Contours from -0.025 to -0.175 in steps of -0.025.

Mode number	Relative amplitude		
	$h/r_d = 3.0$	$h/r_d = 2.0$	$h/r_d = 1.5$
0	0.016	0.199	0.666
1	1.000	1.000	1.000
2	0.001	0.098	0.155
3	0.000	0.008	0.019

TABLE 2. Variation in relative mode amplitude with jet separation, Mode (1, III). $M_j = 1.32$, $M_d = 1.0$, $St = 0.3$, $b = 0.2$.

iterations for the cases considered. The interior coefficients may then be found from (4.2).

For convenience in the present calculations only the pressure field outside the edge of the jet has been determined. Equation (2.3), rewritten in terms of modes that are odd or even about the (x, y)-plane, is used to calculate the pressure. For example, figure 8 shows contours of equal pressure level for the (0, I) mode and $h/r_d = 1.9$. The phase, given by $kx - \omega t$ in (2.4), has been set to zero. It can be seen that the pressure field remains nearly axisymmetric. However, in the region between the two jets there is a loss of axisymmetry. In this region the amplitude of the pressure is nearly uniform and equal to the maximum amplitude achieved at the edge of the jet. The shaded region shows the region of maximum amplitude. This is the case for all the modes that are even about the (x, z)-plane.

A measure of the azimuthal mode content for each mode of instability and type is given by the relative magnitudes of the coefficients F_s and G_s. Table 2 shows how these amplitudes vary with jet separation for the (1, III) mode. For each separation

the $n = 1$ helical mode is dominant. However, for $h/r_d = 1.5$ the $n = 0$ mode amplitude rises to 67% of that of the $n = 1$ mode and the $n = 2$ mode rises to 16% of the $n = 1$ mode.

5. Discussion

The present calculations have shown how the growth rates of instability waves or large structures in the initial mixing region of twin supersonic jets are affected by the jet separation. This interaction is caused by a coupling of the waves' unsteady flow fields even before the time-averaged jet flows have merged. At a given operating condition the mode number and type that is most unstable is a function of the jet separation. However, the quantitative changes in the local growth rates are relatively small until the separation between the jet centrelines approaches the jet diameter: that is $h/r_d \to 1$. Though this may be achieved in theory in the case of the vortex-sheet model, similar calculations for the realistic jet profiles are limited to very small mixing-layer thicknesses. At larger thicknesses the jets merge, rendering the present analysis invalid.

The influence of the jet separation on the eigenvalues can be seen from (3.5)–(3.8). The elements of the matrix $\boldsymbol{A}$ consist of two components: those that depend on h, the jet separation, and those that do not. In fact, the easiest way to construct the matrix elements numerically is to first note that the components that depend on h form a symmetric matrix. The other terms, which only occur on the diagonal, may then be added. As the separation increases, the relative magnitude of the terms that depend on h decreases rapidly, as Hankel functions, relative to the remaining components. Eventually, only the terms given by Γ_n, that occur on the diagonal, are significant. The numerator in (3.6) can be seen to be the dispersion relationship for azimuthal mode number n for a single jet. Thus the single-jet eigenvalues constitute the zeroes of the determinant of matrix $\boldsymbol{A}$ for large jet separations.

It should be noted that the amplitude achieved by an instability wave depends on the integrated growth of the wave with axial distance and the local variation in the shape of the eigenfunction. Thus, relatively small changes in the local growth rate can result in large changes in the eventual amplitude of the wave. For example, using the data shown in figure 5, and assuming that $\mathrm{d}b/\mathrm{d}x$ is given by the single-jet value for the same operating conditions, the amplitude of the (0, III) mode is 24% larger for $h/r_d = 1.9$ compared to $h/r_d = 5.0$ at the location where the jets merge in the former case. However, as mentioned earlier, the rate of spread in the twin-jet case may be decreased by the coflowing, entrained air between the jets. This would increase the relative amplitude at the merger location. In addition, the pressure levels between the jets are much higher in the twin-jet case for mode types I and II, as shown in figure 8. However, it is not clear whether changes of this order of magnitude would be sufficient to explain the observed changes in the near-field pressure levels when the twin jets resonate.

The present analysis has considered only a part of the feedback cycle associated with twin-jet screech. The instability wave's growth into the merged jet region must be determined. In this region the merged jet would resemble more closely a developing rectangular jet. In this case certain normal modes, particularly the flapping mode about the (x, y)-plane, might be enhanced. The interaction between the instability waves and the shock cell structure in the jet that gives rise to the upstream-propagating acoustic wave must then be described. It should be noted that existing theories of jet screech are unable to predict the amplitude even for single

circular jets. Experimentally, the occurrence and amplitude of jet screech are very sensitive to small changes in the detailed geometry of the jet model and laboratory. So a prediction of the occurrence of resonance or its amplitude is extremely difficult.

To assist in the extension of the present calculations to other sections of the feedback loop further experimental data on the aerodynamic development of the twin jets is required. These include the modification to the rate of growth of the jet mixing layers, mean flow contours in the merged jet region, and measurements of the entrained flow between the jets.

Though the present analysis does not answer all the questions regarding the complex phenomenon of twin-jet resonance, it has shown how an instability wave analysis can provide some insight into the interaction of twin supersonic jets.

This work has been supported by NASA Langley Research Center under NASA Grant NAG-1-657. The technical monitor is Dr J. M. Seiner.

REFERENCES

GASTER, M., KIT, E. & WYGNANSKI, I. 1985 Large scale structures in a forced turbulent mixing layer. *J. Fluid Mech.* **150**, 23–39.

MORRIS, P. J. 1988 A note on the effect of forward flight on shock spacing in circular jets. *J. Sound Vib.* **121**, 175–177.

MORRIS, P. J., BHAT, T. R. S. & CHEN, G. 1989 A linear shock cell model for jets of arbitrary exit geometry. *J. Sound Vib.* **132**, 199–211.

PETERSEN, R. A. & SAMET, M. 1988 On the preferred mode of jet instability. *J. Fluid Mech.* **194**, 153–173.

POWELL, A. 1953 On the noise emanating from a two-dimensional jet above the critical pressure. *Aero. Q.* **4**, 103–122.

SEDEL'NIKOV, T. K. 1967 The dispersion relations for multilayer jets and for several jets. In *Physics of Aerodynamic Noise* (ed. A. V. Rimskiy-Korsakov). Moscow: Nauka. (Transl. *NASA* TTF-538, 1969.)

SEINER, J. M., MANNING, J. C. & PONTON, M. K. 1988 Dynamic pressure loads associated with twin supersonic plume resonance. *AIAA J.* **26**, 954–960.

TAM, C. K. W. 1986 On the screech tones of supersonic rectangular jets. *AIAA Paper* 86-1866.

TAM, C. K. W. 1987 Stochastic model theory of broadband shock associated noise from supersonic jets. *J. Sound Vib.* **116**, 265–302.

TAM, C. K. W. & BURTON, D. E. 1984*a* Sound generated by instability waves of supersonic flows. Part 1. Two-dimensional mixing layers. *J. Fluid Mech.* **138**, 249–271.

TAM, C. K. W. & BURTON, D. E. 1984*b* Sound generated by instability waves of supersonic flows. Part 2. Axisymmetric jets. *J. Fluid Mech.* **138**, 273–295.

TAM, C. K. W. & MORRIS, P. J. 1980 The radiation of sound by the instability waves of a compressible plane turbulent shear layer. *J. Fluid Mech.* **98**, 349–381.

TAM, C. K. W. & SEINER, J. M. 1987 Analysis of twin supersonic plume resonance. *AIAA Paper* 87-2695.

TAM, C. K. W., SEINER, J. M. & YU, J. C. 1986 Proposed relationship between broadband shock associated noise and screech tones. *J. Sound Vib.* **110**, 309–321.

TAM, C. K. W. & TANNA, H. K. 1982 Shock associated noise of supersonic jets from convergent–divergent nozzles. *J. Sound Vib.* **81**, 337–358.

TRANTER, C. J. 1968 *Bessel Functions with Some Physical Applications*, Sec. 2.6. English Universities Press.

WLEZIAN, R. W. 1987 Nozzle geometry effects on supersonic jet interaction. *AIAA Paper* 87-2694.